Studies on the Chemistry of Tetraamminezinc(II) Dipermanganate ($[Zn(NH_3)_4](MnO_4)_2$): Low-Temperature Synthesis of the Manganese Zinc Oxide ($ZnMn_2O_4$) Catalyst Precursor

by **István E. Sajó**[a]), **László Kótai***[a]), **Gábor Keresztury**[a]), **István Gács**[a]), **György Pokol**[b]), **János Kristóf**[c]), **Bojan Soptrayanov**[d]), **Vladimir M. Petrusevski**[d]), **Daniel Timpu**[e]), and **Pradeep K. Sharma**[f])

[a]) Chemical Research Center, Hungarian Academy of Sciences, P. O. Box 17, HU-1525 Budapest (e-mail: kotail@mail.chemres.hu)

[b]) Department of Inorganic and Analytical Chemistry, Budapest University of Technology and Economics, Pf. 91, HU-1521 Budapest

[c]) University of Pannonia, Department of Analytical Chemistry, Egyetem u. 10, HU-8200 Veszprém

[d]) University Sv Kiril Metodij, PMF, Institute Hemija, POB 162, Skopje 1001, Macedonia

[e]) Petru Poni Institute of Macromolecular Chemistry, Aleea Gr. Ghica Voda, 41A, Iasi 700487, Romania

[f]) Department of Chemistry, J. N. V. University, Jodhpur, 342005, Jodhpur, India

Tetraamminezinc(II) dipermanganate ($[Zn(NH_3)_4](MnO_4)_2$; **1**) was prepared, and its structure was elucidated with XRD-*Rietveld*-refinement and vibrational-spectroscopy methods. Compound **1** has a cubic lattice consisting of a 3D H-bound network built from blocks formed by four MnO_4^- anions and four $[Zn(NH_3)_4]^{2+}$ cations. The other four MnO_4^- anions are located in a crystallographically different environment, namely in the cavities formed by the attachment of the building blocks. A low-temperature quasi-intramolecular redox reaction producing NH_4NO_3 and amorphous $ZnMn_2O_4$ could be established occurring even at 100°. Due to H-bonds between the $[Zn(NH_3)_4]^{2+}$ cation and the MnO_4^- anion, a redox reaction took place between the NH_3 and the anion; thus, thermal deammoniation of compound **1** cannot be used to prepare $[Zn(NH_3)_2](MnO_4)_2$ (contrary to the behavior of the analogous perrhenate (ReO_4^-) complex). In solution-phase deammoniation, a temperature-dependent hydrolysis process leading to the formation of $Zn(OH)_2$ and NH_4MnO_4 was observed. Refluxing **1** in toluene offering the heat convecting medium, followed by the removal of NH_4NO_3 by washing with H_2O, proved to be an easy and convenient technique for the synthesis of the amorphous $ZnMn_2O_4$.

1. Introduction. – Spinel-type $ZnMn_2O_4$ compounds are widely used materials, *e.g.*, as industrial catalysts in hydrocarbon processing, in chemical and electronic industries, as well as in other areas of technology [1]. The preparation of the reactive solid-state precursors to obtain the highly active defectous $ZnMn_2O_4$ structures at low temperatures might be accomplished by mixing Zn and Mn at atomic level. One of the possible candidates, $[Zn(NH_3)_4](MnO_4)_2$ (**1**) was discovered by *Klobb* [2]. *Müller et al.* [3] studied its IR spectrum and powder X-ray diffractogram, but its detailed structure has not been brought to light yet. Our efforts were directed toward developing a preparation technique to obtain pure compound **1** and to study its structure and properties by means of XRD-*Rietveld*-refinement, vibrational spectroscopy, and thermal methods.

2. Experimental. – *General.* Freshly prepared pure materials were used in all measurements. Solid-state IR spectra: *BioRad-Digilab FTS-45-FT* IR spectrometer in the 4000 – 400 cm^{-1} region and *BioRad-*

Digilab FTS-40-FIR spectrometer in the 400–40 cm^{-1} region; nujol mulls at r.t. Low-temp. IR measurements (−100°): *Perkin-Elmer 2000-FT* IR spectrometer in the 4000–400 cm^{-1} region; AgCl pellets. *Raman* spectra: *Nicolet 950-FT-Raman* spectrometer equipped with a Nd:YAG laser (1064 nm line) for excitation in the 4000–100 cm^{-1} region of *Raman* shifts in a mixture with KBr; during measurements, the compacted powdered sample of **1** was rotated to avoid overheating and decomposition. X-Ray powder diffraction measurements: *Philips PW-1050-Bragg-Brentano* parafocusing goniometer equipped with a secondary beam graphite monochromator and proportional counter; scan recording in step mode by using CuK_α radiation at 40 kV and 35 mA tube power; diffraction-pattern evaluation by full profile fitting techniques; *Rietveld*-refinement parameters: wavelength 1.5406 Å, 2θ range 10–112°, number of data points 5100, profile function *Pearson VII*, $R_{wp} = 0.184$, and weighting scheme $1/y_0$. Thermal studies: *Derivatograph*-type simultaneous thermoanalytical equipment (*Hungarian Optical Works*, Budapest), equipped with a selective H_2O monitor and a gas-titrimetric apparatus (NH_3 was absorbed and determined as static pH titration with 0.1M HCl at pH 5); under N_2; heating rate 2.5°/min. Thermogravimetry (TG)/MS measurements: a *STD-2960* simultaneous DTA/TGA (DTA = differential thermal analysis; TA instruments) and *Thermostar-GSD-200*-Q-MS (*Balzers*) device; 5° heating rate in a He flow. Differential-scanning calometry (DSC): *Mettler-Toledo TA4000* instrument and *Perkin-Elmer Pyris-Diamond* DSC; under N_2; from −50 to 300° and −100 to 25° with 3°/min or 10°/min heating rate, resp. Although accidental explosion of compound **1** did not occur in our experiments, it should be noted that the MnO_4^- complexes of reducing ligands are *potentially hazardous explosives*, and they have to be handled with care.

Tetraamminezinc(2+) Permanganate (1:2) ($[Zn(NH_3)_4](MnO_4)_2$; **1**). A 25% aq. NH_3 soln. (600 ml) was added to 400 ml of an aq. soln. of $ZnSO_4 \cdot 7\ H_2O$ (23 g, 80 mmol), and cooled to +5°. After addition of a sat. (at 5°) aq. $KMnO_4$ soln. (1 l), the mixture was cooled to +2° [2]. The resulting dark purple crystalline solid was filtered off and washed with a small amount of cold H_2O: 4.2 g (13.5%) of **1**. Purple microcrystals.

Tetraamminecopper(2+) Permanganate (1:2) ($[Cu(NH_3)_4](MnO_4)_2$). $[Cu(NH_3)_4](MnO_4)_2$ was prepared according to the method described previously [4].

Manganese Zinc Oxide (Mn_2ZnO_4) ($ZnMn_2O_4$). Compound **1** (4.0 g) was carefully dried at 40° and then mixed with toluene (100 ml). The suspension was refluxed under intensive stirring for 2 h. The solid residue was filtered off, washed successively with H_2O, EtOH, and Et_2O and then dried *in vacuo* at r.t.: black powder (1.1 g, 42%).

3. Results and Discussion. – 3.1. *Synthesis and Hydrolysis of $[Zn(NH_3)_4](MnO_4)_2$* (**1**). Dark purple microcrystalline **1** could be prepared by the reaction of saturated aqueous $[Zn(NH_3)_4]SO_4$ solution and $KMnO_4$ in the presence of an excess of NH_3 by cooling the saturated solution from +5 to +2° (*Eqn. 1*). Higher NH_3 concentration or a larger temperature gradient decreased the purity of the formed **1**. Compound **1** is slightly soluble in H_2O (0.91 g/100 ml at 19°) and stable in the solid state and under dry conditions. However, in wet form, fast decomposition occurs, especially when exposed to light. Compound **1** decomposes in aqueous solution, partially with the formation of MnO_2 and O_2, but (like in the case of the analogous Cu-compound), a temperature-dependent hydrolysis process [4][5] also occurs, and $Zn(OH)_2$ and NH_4MnO_4 are formed (*Eqn. 2*). Evaporation of excess NH_3 at room temperature in vacuum or by mild heating at atmospheric pressure leads to the formation of small needle-like single crystals of NH_4MnO_4 embedded in a brown amorphous matrix[1]).

$$[Zn(NH_3)_4]SO_4\ (aq.) + 2\ KMnO_4\ (aq.) \rightarrow [Zn(NH_3)_4](MnO_4)_2\ (s) + K_2SO_4\ (aq.) \quad (1)$$

$$[Zn(NH_3)_4](MnO_4)_2 + 2\ H_2O \rightarrow Zn(OH)_2 + 2\ NH_3 + 2\ NH_4MnO_4 \quad (2)$$

[1]) The XRD plot of purple crystalline material NH_4MnO_4 is available upon request from *L. K.*

The reaction of *Eqn. 2* is a temperature-dependent hydrolysis reaction of the complex cation [6]. This means dissociation of the $[Zn(NH_3)_4]^{2+}$ ion into Zn^{2+} and NH_3, which is then followed by protonation of a part of the liberated NH_3, namely with the formation of NH_4^+ and OH^- ions. These temperature-dependent equilibrium processes are reversible. However, removal of NH_3 shifts the equilibrium toward the formation of $Zn(OH)_2$ precipitate, thus NH_4^+ and MnO_4^- ions accumulate in the solution. Slow evaporation of this solution under ambient conditions leads to pure single crystalline NH_4MnO_4 identified by the XRD method[1]). Since the partial vapor pressure of NH_3 above the aqueous solution of compound **1** is higher than the vapor pressure of H_2O [6], slow evaporation with mild heating or the removal of NH_3 under vacuum can also be used to complete the reaction of *Eqn. 2*. Due to this reaction, in spite of the existence of H_2O-insoluble $[Zn(NH_3)_2](ReO_4)_2$ [7], the preparation of the analogous MnO_4^- complex, $[Zn(NH_3)_2](MnO_4)_2$, was not succesfull in the partial deammoniation experiments of the aqueous solution of **1**, neither in the room-temperature nor in the higher-temperature deammoniation experiments.

3.2. *X-Ray Studies.* Due to the decomposition reaction during the crystallization periods, our efforts to grow single crystals of **1** were unsuccessful. Therefore, a *Rietveld* refinement of the XRD data was performed (*Fig. 1*[2])). Compound **1** crystallizes in a close packed cubic structure of $[Zn(NH_3)_4]^{2+}$ ions with MnO_4^- anions occupying all the octahedral interstices and half the tetrahedral interstices. Comparison of its lattice parameters with the analogous values of $[Zn(NH_3)_4](ClO_4)_2$ (**2**) [8] and $[Zn(NH_3)_4](ReO_4)_2$ (**3**) [3] is shown in *Table 1*.

Table 1. *Lattice Parameters of Isomorphous* $[Zn(NH_3)_4](MnO_4)_2$ (**1**), $[Zn(NH_3)_4](ClO_4)_2$ (**2**), *and* $[Zn(NH_3)_4](ReO_4)_2$ (**3**)

	1	**2**	**3**
Crystal system	cubic	cubic	cubic
Space group	*F*-43*m* (216)	*F*-43*m* (216)	*F*-43*m* (216)
Lattice constants [Å]	$a = 10.335(10)$	$a = 10.240$	$a = 10.53$
Cell volume [Å^3]	1103.9	1073.7	1167.6
Z	4	4	4
D [g/cm^3]	2.251	2.056	3.743

The main feature of the structure is a three-dimensional Zn–N–H···O–Mn H-bonded network built from block-like structural motifs of 4-4 $[Zn(NH_3)_4]^{2+}$ and MnO_4^- ions. The stoichiometry of this building element indicates that only one of the two MnO_4^- (*Type 1*) takes part in the 3D network. The other MnO_4^- (*Type 2*) is captured in the cavities enclosed by the connection of the tetramer building blocks of the 3D-network (*Fig. 2*[3])). The N···O distances and the strength of the H-bond in the 3D-networks formed either by the *Type 1* MnO_4^- in **1** or by the *Type 1* ClO_4^- in compound **2** are almost the same. The H-bond formed by the *Type 2* MnO_4^- might be only a bit

[2]) Powder X-ray data of $[Zn(NH_3)_4](MnO_4)_2$ (**1**) and $ZnMn_2O_4$ are available upon request from *L. K.*

[3]) The plots of the projection of the structure of $[Zn(NH_3)_4](MnO_4)_2$ (**1**) and of its H-bonds are available upon request from *L. K.*

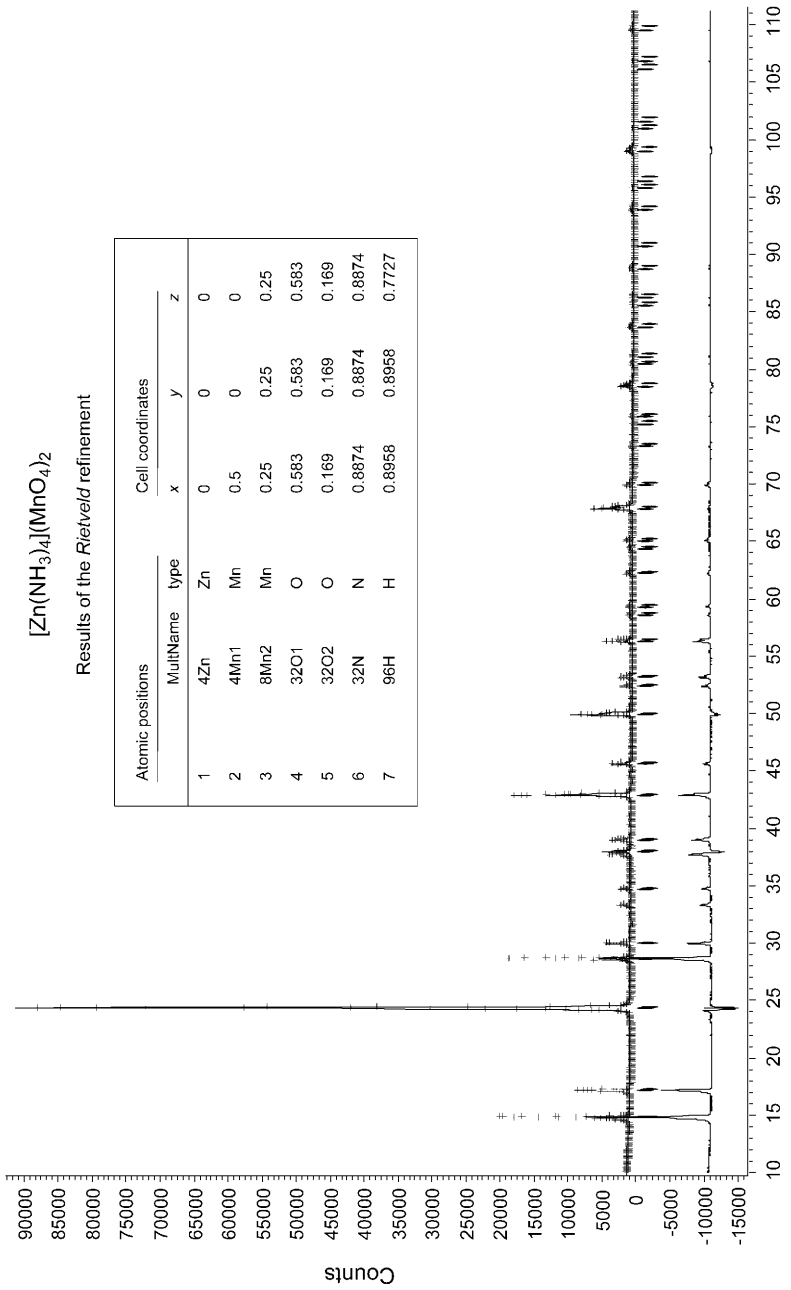

Fig. 1. *Results of* Rietveld *refinement of* $[Zn(NH_3)_4](MnO_4)_2$ (**1**)

stronger than the H-bond formed by the *Type 2* ClO_4^- in the appropriate ClO_4^- salt. The MnO_4^- anions located in the cavities (*Type 2*) are bound with NH_3 H-atoms ($d(O(2)\cdots N) = 3.025$ Å). Therefore, their free rotation is hindered within the cavities, although their freedom is higher than that of the *Type 1* MnO_4^- anions. Thus, refinement can be performed with the best result at higher B_{iso} for O-atoms of *Type 2* MnO_4^- than for O-atoms of *Type 1* MnO_4^-. From the comparison of the N···O atomic distances in **1** and **2** (*Table 2*), it can be concluded that there is no significant difference between the strengths of the H-bonds in **1** and in **2**. The structure and packing of **1** in the solid state can be seen in *Fig. 2*[3]).

Table 2. *Atomic Distances* [Å] *in the Solid Compounds* $[Zn(NH_3)_4](MnO_4)_2$ (**1**) *and* $[Zn(NH_3)_4](ClO_4)_2$ (**2**)

	1	**2** [8]
Zn–N	2.016(24)	2.014
M(1)–O	1.486(22)	1.418
M(2)–O	1.450(20)	1.366
N–H	1.192[a])	1.190
N···O(1)	3.176(35)[b])	3.175
N···O(2)	3.025(33)[b])	3.067

[a]) N–H Atomic distances were only estimated and not refined. [b]) N···O Distances were used to evaluate the strength of H-bonds.

3.3. *Vibrational Spectroscopy Results.* Knowing its crystal structure, the vibrational-spectra analysis of compound **1** can be performed. The result of factor-group analysis for the tetrahedral MnO_4^- anion and the ZnN_4 fragment of the tetrahedral $[Zn(NH_3)_4]^{2+}$ cation is shown in *Table 3*. All four vibrations of these tetrahedral species are *Raman* active, but only the two triply degenerated vibrations are IR active.

Table 3. *Factor-Group Analysis of the* MnO_4^- *Anion and the* ZnN_4 *Fragment of the* $[Zn(NH_3)_4]^{2+}$ *Cation.* Space group: $F4\text{-}3m = T_d^2$ ($Z = 4$, $Z_B = 1$).

Free-ion symmetry	Site symmetry	Factor group	Activity	Assignment
T_d	T_d	T_d		
A_1	A_1	A_1	*Raman*	$\nu_s(MnO_4, ZnN_4)$
E	E	E	*Raman*	δ_E (MnO_4, ZnN_4)
F_2	F_2	F_2	*Raman*, IR	$\nu_{as}(MnO_4, ZnN_4)$
F_2	F_2	F_2	*Raman*, IR	δ_{F2} (MnO_4, ZnN_4)

Permanganate Vibrations. The assignment of the anion vibrations of **1** can be found in *Table 4*[4]). Since there are two crystallographically different MnO_4^- anions in the cubic lattice, *Raman* bands should appear twice for all four (ν_s, δ_E, ν_{F2}, and δ_{F2})

[4]) The results of *ab initio* quantum-chemical frequency calculations of the anion and cation of $[Zn(NH_3)_4(MnO_4)_2$ (**1**) are available upon request from *L. K.*

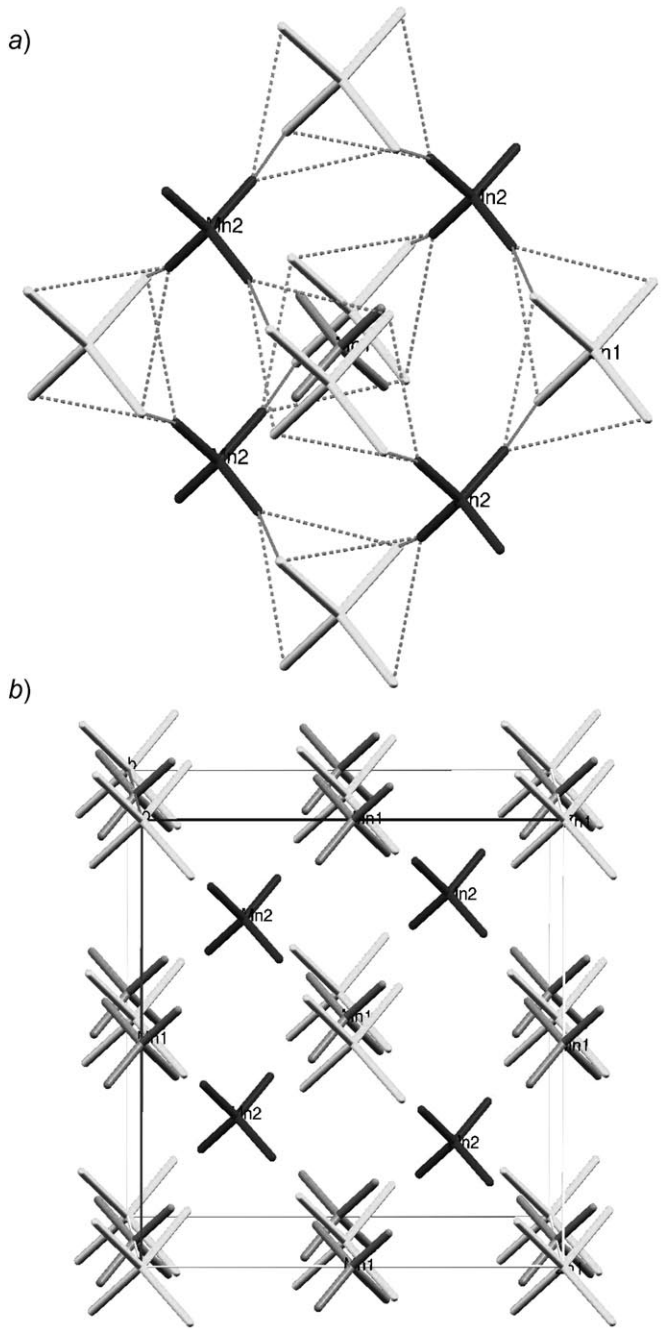

Fig. 2. *Crystal structure of* $[Zn(NH_3)_4](MnO_4)_2$ (**1**). a) *H-Bonds in* **1** *and* b) *packing of* **1**. Light grey tetrahedrons mean the $[Zn(NH_3)_4]^{2+}$ cations; dark grey tetrahedrons mean the two types of MnO_4^- anions (Mn1: cavity-embedded, Mn2: 3D-network-forming MnO_4^-).

Table 4. *Assignment of Vibrational Frequencies of the MnO_4^- Anion Observed in the IR* (Nujol) *and* Raman *Spectra* (KBr) *of [Zn(NH$_3$)$_4$](MnO$_4$)$_2$* (**1**) *at Room Temperature*

	IR (diffuse reflection)		*Raman* (diffuse reflection)	
	$\tilde{\nu}$ [cm^{-1}]	*Type*	$\tilde{\nu}$ [cm^{-1}]	*Type*
$\nu_s(MnO_4)$	836*w*	*2*[a])	841v*s*	*1*[b])
			836v*s*	*2*[a]
δ_E (MnO_4)	345*m*	*2*[a])	346*m*	*2*[a])
			342 (sh)	*1*[b])
$\nu_{as}(MnO_4)$	910v*s*		914 (sh)	
	900v*s*		908*m*	
			903*m*	
			897*m*	
			892 (sh)	
δ_{F2} (MnO_4)	388*w* (sh)		388*m*	
	381*m*		381 (sh)	
Combination bands				
$\nu_s + \nu_{as}$[c]) (MnO_4)	1749*w*			
$\nu_s + \nu_{as}$[c]) (MnO_4)	1728*w*			

[a]) Cavity-embedded type of MnO_4^- anions (tentative assignment). [b]) 3D-Network-bound type of MnO_4^- anions (tentative assignment). [c]) The components of the ν_{as} stretching.

vibrational normal modes. Since the degeneration of the F_2 bands in this symmetric crystallographical environment does not cease, splitting of the ν_{as} asymmetric stretching bands into $3+2$ bands (or into 2×3 bands with overlapping two neighboring bands) is an unusual phenomenon. An inconsistency was found in the IR spectra either (*Figs. 3* and *4*). Like in the case of the corresponding ClO_4^- complex **2**, both of the forbidden IR bands (ν_s and δ_E) appear as a *singlet* in the IR spectrum. This and the splitting of at least one of the triply degenerated ν_{as} bands into three components in the *Raman* spectrum show a lowering of symmetry of at least one type of the MnO_4^- anion environments. The lowering of symmetry may appear in case of the other type of MnO_4^- as well, due to the splitting of both kinds of the ν_{as} *Raman* bands; however, only one kind of the forbidden IR bands appears. There are several possible reasons for the appearance of the forbidden IR bands of tetrahedral oxo anions [9]. One of them is a dynamic lattice distortion as it was supposed in the case of compound **2** [8], or some orientational effect which was observed several times in N–H H-bonded compounds, *e.g.*, in NH_4ClO_4 [10]. Although both the dynamic lattice distortion and the MnO_4^- orientation depend on the temperature, but with opposite sign. Decreasing the temperature can freeze one orientation, and this should increase the intensity of the forbidden band. In the case of a dynamic lattice distortion, however, the decreasing temperature decreases the extent of distortion, because the anisotropic thermal motions are slowing down. Based on these considerations, liquid-N_2-temperature IR studies were performed to study the effect of temperature on the intensity of the forbidden ν_s(Mn–O) bands of compound **1**. To disclose the effect of possible phase transitions on the low-temperature IR-spectral features, a low-temperature differential-scanning-calometry (DSC) study was also performed. The DSC results confirmed the absence of any phase transitions. Since the decrease of temperature affects the band widths, the integrated intensities of each

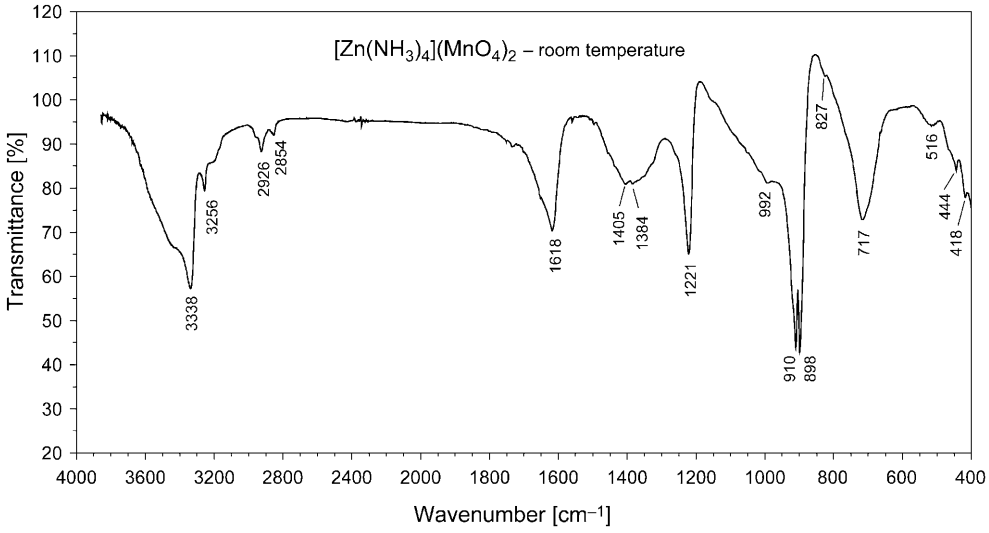

Fig. 3. *Room-temperature IR spectrum of* $[Zn(NH_3)_4](MnO_4)_2$ (**1**) *in AgCl matrix*

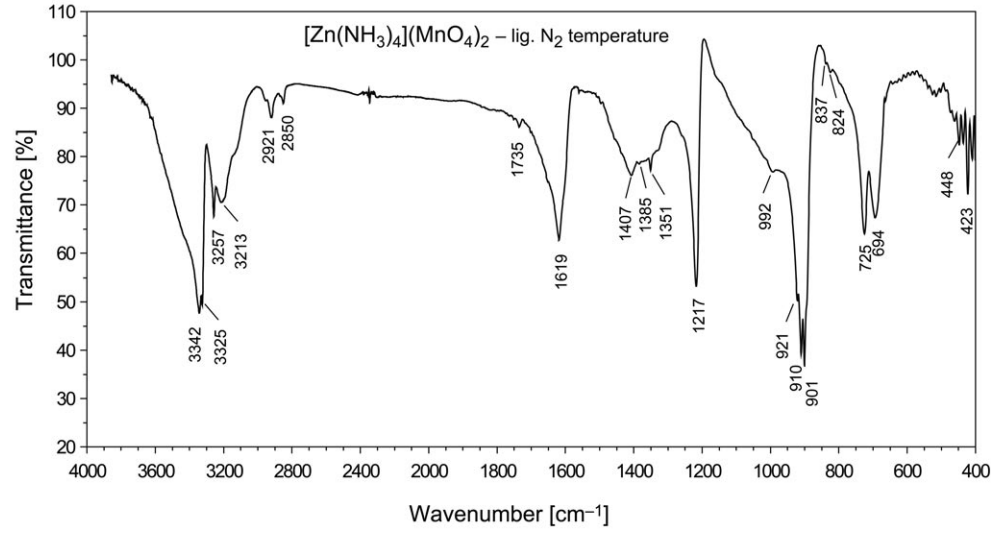

Fig. 4. *Low-temperature* ($-100°$) *IR spectrum of* $[Zn(NH_3)_4](MnO_4)_2$ (**1**) *in AgCl matrix*

group of bands were calculated for each spectrum, and the intensity ratios $I(\nu_{as}; Mn-O)/I(\nu_s; Mn-O)$ were compared. The analogous Cu-complex $[Cu(NH_3)_4](MnO_4)_2$ (**4**) [4] has no dynamic lattice distortion or favored MnO_4^- orientation; therefore, compound **4** was also studied to compare the effect of cooling on the intensity ratios of the bands. The change in the ratio $I(\nu_{as}; Mn-O)/I(\nu_s; Mn-O)$ of **4** was less than 20% during cooling from room temperature to liquid-N_2 temperature

(*Table 5*). In the case of **1**, however, this change was more than 150%. Since the intensity of the ν_s band increases with decreasing temperature, the dynamic lattice distortion as a possible reason for the appearance of the forbidden IR and splitting of the degenerated *Raman* bands seems to be less probable than the effect of the MnO_4^- anion orientation. Based on this consideration, the forbidden ν_s and δ_E IR bands probably belong to the cavity-embedded MnO_4^- (*Type 2*). The appropriate *Raman* bands of this type of MnO_4^- were assigned on the basis of the wavenumbers of the given *Raman* and the forbidden IR bands. The other *Raman* bands in each pair of bands were attributed to the 3D network-bound MnO_4^- (*Type 1*). Unambiguous assignment of the F_2 bands of each MnO_4^- type was not possible because the ν_{as} band in the low-temperature IR spectrum was split into only three bands (901, 910, and 921), and δ_{F2} was out of the measurement range (4000 – 400 cm^{-1}) of the low-temperature IR device.

Table 5. *Comparison of Integrated Intensities* I(*ν*) [%] *of Room-Temperature and Liquid-N_2-Temperature Forbidden $\nu_s(Mn-O)$ IR Bands of $[Zn(NH_3)_4](MnO_4)_2$* (**1**) *with the $\nu_s(Mn-O)$ of the Analogous $[Cu(NH_3)_4](MnO_4)_2$* (**4**) *in AgCl Matrix*

	1		**4**	
	25°	– 100°	25°	– 100°
$I(\nu_s)$	0.052	0.133	0.684	0.839
$I(\nu_{as})$	14.350	14.377	35.395	36.283
$I(\nu_{as})/I(\nu_s)$	276 (253%)	109 (100%)	51.7 (119%)	43.4 (100%)

Two combination bands were also assigned to the MnO_4^- anion. These are the $\nu_s + \nu_{as}$ bands, when two components of ν_{as} gave separated combinations. These bands were assigned to the MnO_4^- anion because similar bands and band structures were also observed in the diffuse-reflection IR spectra of $KMnO_4$ and NH_4MnO_4 [11].

Tetraamminezinc(II) Cation Vibrations. The $[Zn(NH_3)_4]^{2+}$ complex cation has 17 atoms, and there are 11 *Raman*-active ($3A_1 + 8E$) and 21 (F_2) IR- and *Raman*-active bands that can be taken into consideration among the 45 possible vibrational modes. All vibrations belonging to the coordinated NH_3 are IR- and *Raman*-active. The assignment of the vibrational bands belonging to the complex cation are given in *Table 6*. The bands in the IR spectra at 421, 388 (*Table 4*), and 381 cm^{-1} (*Table 4*) may belong to any of the $\nu_s(ZnN_4)$, $\nu_{as}(ZnN_4)$, and $\delta_{F2}(MnO_4)$ modes. To assign these bands, *ab initio* quantum-chemical calculations were performed on the MnO_4^- and $[Zn(NH_3)_4]^{2+}$ ion[4]). Also the IR data of **1** were compared with those of the analogous $[Zn(NH_3)_4](ClO_4)_2$ (**2**) and $[Zn(NH_3)_4](ReO_4)_2$ (**3**) complexes, and of an isotope-substituted derivative, $[Zn(^{15}NH_3)_4](ReO_4)_2$ [3][7][8][12].

A band appearing at 421 cm^{-1} was observed in the spectra of each isomorphous compound **1**–**3** [3][8][12]. Since all of the four normal modes of the ClO_4^- were assigned, and $\delta_{F2}(ClO)$ appeared at 630 cm^{-1} and $\delta_{F2}(MnO_4)$ below 400 cm^{-1} (*Table 4*), this band definitely belonged to one of the Zn–N vibrations. The quantum-chemical calculations (DFT//BLYP/TZCVP) showed that the value of the $\nu_s(ZnN_4)$ frequency is higher than the value of the $\nu_{as}(ZnN_4)$ frequency. Although $\nu_s(ZnN_4)$ is IR-inactive and should not be observed, it was detected as a weak band at

Table 6. *Assignment of* $[Zn(NH_3)_4]^{2+}$ *Ion Frequencies in the IR* (Nujol) *and* Raman *Spectra* (KBr) *of Compound* **1** *at Room Temperature*

	$\tilde{\nu}$ [cm^{-1}]		
	Species	IR (diffuse reflection)	*Raman* (1064 nm)
$Zn-NH_3$ Vibrations:			
$\nu_s(NH)$	A_1	3253*m*	3258v*w*
			3163v*w*
$\delta_s(NH)$	A_1	1219*s*	–
$\nu_s(ZnN_4)$	A_1	–	–
$\nu_{as}(NH)$	E	3329v*s*	3326v*w*
$\delta_E(NH)$	E	1612*m*	–
$\rho_r(NH)$	E	716*w*	–
		690*w*	695v*w*
Zn–N Vibrations:			
$\nu_s(ZnN_4)$	A_1	451*w*	–
$\delta_E(ZnN_4)$	E	232*w*	–
$\nu_{as}(ZnN_4)$	F_2	421*m*	426*w*
$\delta_{F2}(ZnN_4)$	F_2	179*s*	–
Combination and overtone bands:			
$2\delta_E(NH)$		3193	–
$\rho_r+\rho_r(NH)$[a])		1401	–
$2\rho_r(NH)$[a])		1384	–
$2\nu_{as}(ZnN_4)$		848	–

[a]) The components of the ρ_r N–H rocking stretching.

451 cm^{-1} (the band at 421 cm^{-1} is believed to arise from $\nu_{as}(ZnN_4)$). The forbidden $\nu_s(ZnN_4)$ band also appeared at 432 and 411 cm^{-1} in the spectra of the isomorphous compounds **2** and **3**, respectively. However, only one band (ν_{as} at 403 cm^{-1}) was found in the IR spectra of $[Zn(^{15}NH_3)_4](ReO_4)_2$, but its *Raman* spectrum contained two bands (411 and 403 cm^{-1}), which were unambiguously assigned to the appropriate *Raman*-active $\nu_s(ZnN_4)$ and $\nu_{as}(ZnN_4)$ modes [12]. Appearance of the forbidden $\nu_s(ZnN_4)$ and $\delta_E(ZnN_4)$ bands in the IR spectrum of **1** is the consequence of the interaction between the encaged MnO_4^- (*Type 2*) and the NH_3 H-atoms of the cations. The $\delta_E(ZnN_4)$ was assigned to the band at 232 cm^{-1}, which is near to the 221 cm^{-1} band of compound **2** [8]. The IR-active asymmetrical deformation band $\delta_{F2}(ZnN_4)$ was observed at 179 cm^{-1} as a strong and broad band, located close to the appropriate value of **2** (178 cm^{-1}) [8] and **3** (191 cm^{-1}) [3]; for the isotope-labelled ($^{15}NH_3$) analogous ReO_4^- complex, this band appeared at 174 cm^{-1} [12]. Generally, the IR absorptions of **1** measured by *Müller et al.* [3] in KBr were located at higher frequencies than in our spectrum obtained in the diffuse-reflection mode. The low-temperature IR measurements of **1** in AgCl showed four bands (462, 448, 436, and 423 cm^{-1}) which probably arose from the *singlet* of $\nu_s(ZnN_4)$ and a *triplet* of $\nu_{as}(ZnN_4)$. The *Raman* spectra of **1** at room temperature contained only one assignable band ($\nu_{as}(ZnN_4)$ at 426 cm^{-1}, weak); the other three *Raman*-active modes could not be detected due to their low intensity.

Based on these considerations and the quantum-chemical calculations (G94//B3LYP/6-311G and DFT//BLYP/TZVP), the other two bands at 388 and 381 cm^{-1} do

not belong to the ZnN_4 vibrations but may belong to the two different MnO_4^- anions and can be assigned as a pair of the $\delta_{F2}(MnO_4)$ bands (see above, *Table 4*).

3.4. *Thermal Studies.* To avoid explosion-like decomposition, Al_2O_3 was added to **1** (10% of **1** in α-Al_2O_3) to perform thermogravimetry (TG)/MS measurements. Decomposition under inert atmosphere occurred in $2+1$ steps. On the basis of mass-loss data (residue was 64.20%), the amorphous product was estimated to have a $[ZnO + Mn_2O_3]$ formula (theoretical value, 64.40%). The first decomposition step occurred at 107°; however, the decomposition peak temperature varied in the 100–130° range depending on the heating rate. This temperature was lower than the deammoniation temperature of the analogous ReO_4^- salt **3** (150–195°, at which the intermediate $[Zn(NH_3)_2](ReO_4)_2$ complex [7] was formed). The thermo-gas titrimetric investigation indicated that 2 mol of NH_3 were released in the first decomposition step, and no further NH_3 formation in the second or third step was observed. The unambiguous features of this decomposition process were the formation of H_2O in the first two steps and the lack of O_2 evolution in the entire thermal-decomposition process. Mainly N_2O and its fragmentation products were detected in the second step, although some N_2 and other NO_x by-products could also be detected in the other decomposition steps, as also observed in the case of compound **4** [4]. The weight loss in the third step was 5.4%, which can be attributed to the decomposition of some previously formed by-products or $ZnMn_2O_{4+x}$ nonstoichiometric phases. IR Studies performed on the white crystals obtained from the aqueous extract of the X-ray amorphous thermal-decomposition intermediates formed in the first decomposition step unambiguously confirmed the formation of NH_4NO_3. The final decomposition product was heated up to 500°. XRD of the residue showed only the presence of the tetragonal modification of $ZnMn_2O_4$. Summarizing these results, the main decomposition process of compound **1** can be illustrated with *Eqn. 3*. Dissimilarly from the corresponding ReO_4^- salt **3** [7], the diammine complex $[Zn(NH_3)_2](MnO_4)_2$ did not form. The second decomposition step (T_{peak} 231°) was a $ZnMn_2O_4$-catalyzed decomposition reaction of NH_4NO_3 (*Eqn. 4*).

$$[Zn(NH_3)_4](MnO_4)_2 \rightarrow ZnMn_2O_4 + NH_4NO_3 + 2\,NH_3 + H_2O \quad (3)$$

$$NH_4NO_3 \rightarrow N_2O + 2\,H_2O \quad (4)$$

Since the thermal-decomposition temperature of the NH_4NO_3 formed according to *Eqn. 3* was lower than the decomposition temperature of pure NH_4NO_3 (260°) [13], and not only N_2O but other NO_x products were also formed, the $ZnMn_2O_4$ probably catalyzed this decomposition reaction. DSC Studies showed that all decomposition steps were exothermic. The reaction heat ΔH was -169 kJ/mol in the first step (*Eqn. 3*), which was lower than the appropriate reaction heat of compound **4** ($\Delta H = -290$ kJ/mol). The reaction heat of the second decomposition step (*Eqn. 4*) could not be determined because of the explosion-like decomposition of NH_4NO_3. The explosion-like decomposition of NH_4NO_3 also confirmed the suggested catalytic effect of the formed $ZnMn_2O_4$.

The lack of an endothermic effect of NH_3 liberation from the complex cation $[Zn(NH_3)_4]^{2+}$ indicated that the exothermic solid-phase quasi-intramolecular redox reaction between the NH_3 ligand and the MnO_4^- anion started before the deammo-

niation step of the complex cation. Due to this reaction, the $[Zn(NH_3)_2](MnO_4)_2$ complex could not be prepared by partial deammoniation of complex **1**. Since $[Zn(NH_3)_2](ReO_4)_2$ was prepared in this way [7], the higher redox activity of MnO_4^- may be one of the reasons for this redox reaction. On the other hand, this redox reaction provided a possibility for the preparation of $ZnMn_2O_4$-type materials. To control the reaction rate, the use of toluene as a liquid heat-convecting medium (the boiling point of toluene is almost the same as the decomposition temperature of **1**) proved to be suitable. After refluxing for 2 h, the filtered residue was washed with H_2O, then dried, and finally heated up to 500°. The crystallization process of $ZnMn_2O_4$ (tetragonal modification) as a function of the temperature was monitored by XRD (see *Fig. 5*[2])). *Fig. 5* shows that the formal $[ZnO + Mn_2O_3]$ product formed during thermal decomposition consisted of a highly defectous amorphous $ZnMn_2O_4$ spinel-like compound which could be crystallized by heat treatment up to 500°. The amorphous decomposition product is a potential catalyst and can be applied as an additive in various industrial processes and products [1].

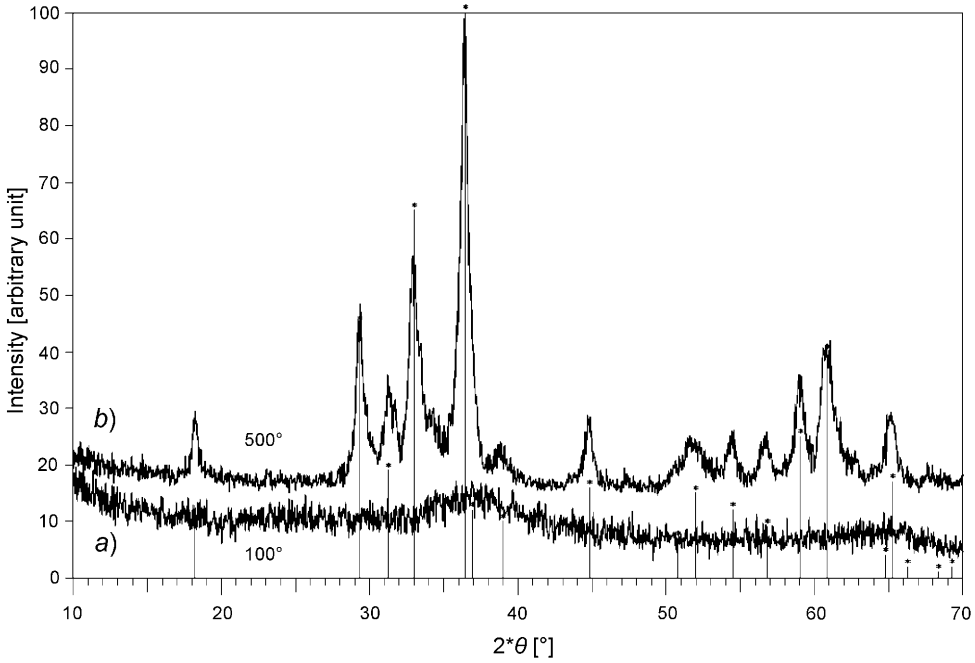

Fig. 5. *XRD of* a) *the amorphous formal* $[ZnO + Mn_2O_3]$ *product formed from* $[Zn(NH_3)_4](MnO_4)_2$ (**1**) *at 100° in toluene, and* b) *tetragonal* $ZnMn_2O_4$ *formed at 500°*

4. Conclusions. – $[Zn(NH_3)_4](MnO_4)_2$ (**1**) has a cubic lattice consisting of a 3D H-bound network of the building blocks of 4-4 $[Zn(NH_3)_4]^{2+}$ cations and MnO_4^- anions. The residual MnO_4^- anions are located in crystallographically different environments. The temperature-dependent orientation of the MnO_4^- anion is the reason for the appearance of forbidden IR bands and splitting of the degenerated *Raman* bands. The

presence of the H-bonds between the complex cation and the anion results in a low-temperature intramolecular redox reaction with the formation of NH_4NO_3 and an amorphous highly defectous $ZnMn_2O_4$ around 100°. In solution-phase deammoniation, a temperature-dependent hydrolysis process occurs, and $Zn(OH)_2$ and NH_4MnO_4 are formed. Dissimilarly from the analogous ReO_4^- complex, $[Zn(NH_3)_2(MnO_4)_2]$ cannot be obtained by thermal deammoniation of compound **1**. This is due to the higher redox activity of the MnO_4^- anion. Thermal treatment of compound **1** in toluene as heat-convecting medium leads to an easy and controlled preparation of the highly defectous amorphous $ZnMn_2O_4$ catalyst precursor.

5. Supplementary Material. – The following supplements are available upon request from *L. K.:* Far-IR spectrum of $[Zn(NH_3)_4](MnO_4)_2$ (**1**) in nujol. *Raman* spectrum of **1** in KBr. CIF File of the X-ray study of **1**. IR Spectra of the white crystals (NH_4NO_3) isolated from the aq. extract of the product formed in the first decomposition step of **1**. TG Results of **1** under He (5°/min; diluted with Al_2O_3). TG/DTG/DTA and H_2O-Detector study of **1** under N_2 (5°/min; diluted with Al_2O_3). TG/MS Plot for NH_3 (and its fragments) evolved during thermal decomposition of **1**. See also *Footnotes 1–4*.

The authors wish to thank Dr. *Béla Pukánszky* for the high-temperature-range DSC measurements.

REFERENCES

[1] Y. Sakata, C. A. van Tol-Koutstaal, V. Ponec, *J. Catal*. **1997**, *169*, 13; I. V. Kryslova, G. N. Pirogova, N. M. Panich, *Russ. Chem. Bull.* **1997**, *46*, 1543; Y. Hui, H. Yang, Y. Lu, N. Li, B. Li, *J. Power Sources* **1996**, *62*, 223; A. Maltha, S. C. van Wermeskeren, B. Brunet, V. Ponec, *J. Mol. Catal*. **1994**, *93*, 305.
[2] T. Klobb, *C. R. Acad. Sci*. **1886**, *103*, 384; T. Klobb, *Bull. Soc. Chim. Fr.* [3] **1890**, *3*, 508.
[3] A. Müller, I. Böschen, E. J. Baran, P. J. Aymonino, *Monatsh. Chem*. **1973**, *104*, 836.
[4] L. Kótai, K. K. Banerji, I. E. Sajó, J. Kristóf, B. Sreedhar, S. Holly, G. Keresztury, A. Rockenbauer, *Helv. Chim. Acta* **2002**, *85*, 2316.
[5] L. Kótai, T. Horváth, K. Szentmihályi, A. Keszler, *Transit. Metal Chem*. **2000**, *25*, 293.
[6] L. Kótai, I. Gács, B. Kazinczy, I. E. Sajó, *Transit. Metal Chem*. **2003**, *28*, 292.
[7] M. C. Chakravorti, M. B. Sarkar, *Transit. Metal Chem*. **1982**, *7*, 19.
[8] H. Hillebrecht, G. Thiele, A. Koppenhoefer, H. Vahrenkamp, *Z. Naturforsch., B* **1994**, *49*, 1163.
[9] A. Hezel, D. Ross, *Spectrochim. Acta* **1966**, *22*, 1949.
[10] C. S. Choi, H. J. Prask, *J. Chem. Phys.* **1974**, *61*, 3523.
[11] L. Kótai, Gy. Argay, S. Holly, A. Keszler, B. Pukánszky, K. K. Banerji, *Z. Anorg. Allgem. Chem.* **2001**, *627*, 114.
[12] C. Tellez, *Spectrosc. Lett.* **1988**, *21*, 871.
[13] 'Römpps Chemie-Lexikon', 7. Auflage, Kosmos-Verlag, Stuttgart, 1972.

Received April 7, 2008